Specificity and mechanism of 1,6 hexanediol-induced disruption of nuclear transport

Elizabeth C. Riquelme Barrientos[a], Tegan A. Otto[a], Sara N. Mouton[a], Anton Steen[a], Liesbeth M. Veenhoff[a]

[a]European Research Institute for the Biology of Ageing, University of Groningen, University Medical Center Groningen, 9713 AV Groningen, The Netherlands

To whom correspondence should be addressed: l.m.veenhoff@rug.nl

Keywords: Nuclear Pore Complex, 1,6-hexanediol, Nuclear Transport Receptors, nuclear transport, aliphatic alcohol, liquid-liquid phase separation, baker's yeast.

ABSTRACT

Selective transport through the nuclear pore complex (NPC) depends on the dynamic binding of the intrinsically disordered components of the NPC, the FG-nups, with each other and with nuclear transport receptors (NTRs). Hydrophobic interactions with the phenylalanines of FG-nups are critical for this dynamic binding. 1,6-hexanediol (1,6HD), is an aliphatic alcohol that interferes with hydrophobic interactions. Here we assessed the specificity and mechanism by which 1,6HD disrupts the permeability barrier of NPCs in live baker's yeast cells. Exposure to 1,6HD (10 min, 0-5%) leads to gradual loss of the NPC permeability. This is likely a direct effect on the nuclear transport machinery as cell viability, the pH and ATP levels in the cytosol, as well as the appearance of mitochondria, Golgi, peroxisomes, ER, vacuoles, plasma membrane, nucleolus, secretory pathway and stress granules are not notably changed. There are however effects on the cytoskeleton and Hsp104 to be noted. While 1,6HD treatment does not lead to dissociation or degradation of NPC subunits, a massive relocation of multiple NTRs from NPCs does occur. This displacement quantitatively correlates with the increased passive permeability of NPCs. The loss of NTRs and associated cargo will present a major change in the macromolecular crowding and composition and hence the physicochemical properties of the central channel. We conclude that 1,6HD provides a surprisingly specific intervention to temporarily permeate NPCs and we present evidence that the mechanism includes release of NTRs from the NPCs.

INTRODUCTION

The Nuclear Pore Complex (NPC) is the sole gate between the nucleus and cytosol. The central channel of NPCs is lined with intrinsically disordered phenylalanine-glycine rich nucleoporins, the FG-nups, and it hosts many nuclear transport receptors (NTRs) (Dultz et al. 2022; Hampoelz et al. 2019; Wing, Fung, and Chook 2022; Fernandez-Martinez and Rout 2021). The NTRs bind their cargo and shuttle them through the channel by transiently binding the FG-nups (Paci, Caria, and Lemke 2021; Wing, Fung, and Chook 2022; Bayliss, Littlewood, and Stewart 2000). For the NTR Importinβ it was shown that besides a fraction that is shuttling cargo between the cytoplasm and nucleus, there is also a fraction that is more stably associated with NPCs (Lowe et al. 2015; Kapinos et al. 2014). In addition to NTRs also cargo and non-cargo are present in the NPC. In isolated yeast NPCs, 15,6 MDa worth of NTRs and 10,4 MDa worth of cargo add significantly to the 52,3 MDa mass of actual NPC subunits (Kim et al. 2018). The central channel of the nuclear pore complex is thus a highly crowded and complex environment where the joint presence of NTRs, FG-nups and cargo creates an environment that allows fast and selective transport.

The exact structure of the central channel has remained elusive because experimentally probing its behaviour in living cells is challenging. Our knowledge about the behaviour of the FG-nups and NTRs is inferred from, amongst others, imaging detergent-perforated or live cells (Chowdhury, Sau, and Musser 2022; Schnell, Tingey, and Yang 2022; Mattheyses et al. 2010; Yu et al. 2022), AFM measurements on nuclear envelopes (Sakiyama et al. 2016), transport measurement in biomimetic NPCs (Jovanovic-Talisman et al. 2009; Fisher et al. 2018; Kowalczyk et al. 2011), surface anchored FG-nups (Kapinos et al. 2014) or from probing the structural conformation of purified FG-nups or FG-nup fragment preparations (Frey, Richter, and Görlich 2006; Celetti et al. 2020; Ader et al. 2010; Hayama et al. 2018; Sparks et al. 2018). These experimental studies, together with computational strategies (Davis, Ford, and Hoogenboom 2022; Zheng and Zilman 2023; Isgro and Schulten 2007; Popken et al. 2015; Ghavami et al. 2014), have resulted in a number of models explaining the fast and selective transport through the NPC (Dultz et al. 2022; Hampoelz et al. 2019; Wing, Fung, and Chook 2022; Fernandez-Martinez and Rout 2021; Hoogenboom et al. 2021; Huang and Szleifer 2020). All models agree that the phenylalanines of the FG-repeat regions that are engaging in hydrophobic interactions, as well as the intrinsically disordered nature of the FG-nups, are key parameters. They enable the highly dynamic intra- and inter-chain hydrophobic interactions between FG-repeat regions and with the hydrophobic grooves on the surfaces of NTRs. In the Kap-centric models the slow exchanging pool of NTRs are proposed to be important to create the proper barrier function (Kapinos et al. 2017; Kalita et al. 2022; Fragasso et al. 2022).

Early experiments using aliphatic alcohols pointed to the importance of hydrophobic interactions for import into nuclei of permeabilized cells (Ribbeck and Görlich 2002) and in live yeast cells (Shulga and Goldfarb 2003). Early experiments in permeabilized HeLa cells showed that selective transport of fluorescent reporters (MBP or IBB-MBP) was abrogated in the presence of hexane-1,2-diol but not by the less hydrophobic hexane-1,2,3-triol (Ribbeck and Görlich 2002). In live yeast cells it was observed that the nuclear accumulation of GFP fused to a classical nuclear localisation signal (NLS) was lost upon addition of alcohols and the extend of equilibration was dependent on the hydrophobicity of the alcohol (Shulga and Goldfarb 2003). Biochemical studies using purified FG-repeat fragments show that some of them are cohesive and that their interactions are disrupted by 1,6HD (Patel et al. 2007; Schmidt and Görlich 2015). Also, within the yeast cytosol such overexpressed fragments form foci that are dispersed by 1,6HD (Patel et al. 2007). Lastly, 1,6 HD was shown to increases the diameter of NPCs in *Xenopus* oocyte nuclear envelope preparations (Jäggi et al. 2003). Most dramatically, in the context of mutant NPCs that lack the inner ring nucleoporins Nup170 or Nup188, 1,6HD can even lead to loss of FG-nups from these NPCs (Shulga and Goldfarb 2003; Onischenko et al. 2017). The effect of hexanediol in the above studies was attributed to a reversible disruption of inter-FG repeat cohesion. However, as also the interactions between NTRs and FG-nups are based on hydrophobic interactions, hexanediol will likely also take effect here. Illustrative for the high surface hydrophobicity of NTRs, is their strong binding to a phenyl sepharose chromatography column yielding highly enriched fractions from HeLa cell extracts (Ribbeck and Görlich 2002). Jointly these studies support the importance of hydrophobic interaction for nuclear transport, and the potential of 1,6 HD to disrupt those.

Unrelated to nuclear transport, 1,6HD has also been widely used to dissolve liquid-liquid phase separated compartments in cells and to dissolve condensates in *in vitro* studies. With aggregation-prone peptides, the alcohol dissolves hydrogels (Molliex et al. 2015; Kroschwald, Maharana, and Simon 2017; Shi et al. 2017) but not fibers (Lin et al. 2016; Van Lindt et al. 2022). In cells, the interpretation of effects of 1,6HD are more difficult (Kroschwald, Maharana, and Simon 2017) and depending on the cell type, growth condition and the concentration and length of treatment different results may be obtained. There are many examples of discrepancies in the literature; only one example is the organization of actin and tubulin. While some reports show that they are affected by 1,6HD (Wheeler et al. 2016; Kroschwald, Maharana, and Simon 2017), others report that microtubules are unaffected (Lin et al. 2016).

From the above, the question arises how specific the effects of 1,6HD on nuclear transport are and, whether they are based on a loss of cohesion between the FG-repeat regions, or between FG-nups and NTRs, or both. Here, we probe the impact of 1,6HD on nuclear transport by measuring the effects on passive transport, on NTR-facilitated import and export, and on the cellular localisation of Nups

and NTRs. We also assess a large number of possible indirect effects of 1,6HD, namely cell viability, the pH and ATP levels in the cytosol, and the appearance of mitochondria, Golgi, peroxisomes, ER, vacuoles, plasma membrane, nucleolus, secretory pathway, stress granules, the cytoskeleton and Hsp104 foci. Our data support that 1,6HD provides a surprisingly specific intervention to temporarily increase the passive permeability of NPCs by the release of NTRs from the NPC.

RESULTS

Disruption of the permeability barrier of NPCs by 1,6 hexanediol

Previous reports already showed that 1,6HD disrupts the permeability barrier of NPCs in yeast cells (Shulga and Goldfarb 2003; Patel et al. 2007). We add to this work and provide a quantitative assessment of the impact of 1,6HD on passive nuclear entry of large reporters and NTR-mediated transport of GFP-NLS and GFP-NES reporters in yeast. To assess passive nuclear entry, the MG5 reporter, composed of a Maltose Binding Protein and 5 GFPs is used. MG5 has a molecular weight of 177 kDa and is excluded from the nucleus in wild type cells (Popken et al. 2015). Mid exponential growing cells were exposed for 10 minutes to zero, 0.625, 1.25, 2.5 or 5% 1,6HD, or to the less hydrophobic alcohol 2,5 hexanediol (2,5HD). The steady state distribution of the GFP-reporters was calculated by taking the ratio of the fluorescence measured in the nucleus and the cytosol (the N/C ratio). The permeability of the NPCs for entry of MG5 increased gradually with increasing concentrations of 1,6HD (Fig 1A) indicating that NPCs became more permeable for this large protein. 1,6HD had a stronger effect on the passive permeability of NPCs than 2,5HD, as MG5 remains properly excluded from the nucleus, even at a concentration of 5% 2,5HD (Fig 1A).

To assess active import and export, GFP with a classical NLS (GFP-cNLS) and GFP-NES reporters are used. The balance between Kap60/Kap95-facilitated import of GFP-cNLS and its passive efflux leads to nuclear accumulation. Similarly, the balance of CRM1-facilitated export of GFP-NES and its passive influx leads to a steady-state nuclear exclusion. The import and export reporters showed a gradual decline in nuclear accumulation and exclusion, respectively, with increasing 1,6HD concentrations (Fig 1B,C). This loss of nuclear compartmentalisation could solely be the consequence of the increased passive permeability (Fig 1A), but could additionally be the result of a decrease in the active transport rates. As for passive transport 1,6HD had a stronger effect for active transport than 2,5HD, as higher concentrations of 2,5HD were needed to decrease the compartmentalisation of GFP-NLS and GFP-NES (Fig 1B,C). From this we conclude that exposure of live yeast cells to 1,6HD (10 min, 0-5%) leads to a gradual loss of the permeability barrier of NPCs.

132

133 **On the specificity of 1,6HD towards disrupting nuclear transport**

134 The question if the increased NPC permeability after exposure to 1,6HD is a direct consequence of an
135 altered nuclear transport system, or rather a consequence of indirect effects on the cell's physiology,
136 is pertinent. Indeed, depending on the exposure time and concentration 1,6HD may well have
137 pleotropic effects in cells, as also previously discussed (Kroschwald, Maharana, and Simon 2017).
138 Using the set concentration of 5% 1,6HD, we assessed all aspects of cell physiology that we deemed
139 relevant and could assess. First, we treat the cells for 10 or 30 min with 5% 1,6HD or 2,5HD and
140 observed no effects on cell viability (Fig 2A). Then, we assessed if 10 min exposure to 5% 1,6HD leads
141 to changes in free ATP levels or cytosolic pH, using fluorescence-based sensors (Imamura et al. 2009;
142 Miesenböck, De Angelis, and Rothman 1998). Our rationale for testing these was that ATP and pH
143 levels could change when cells are experiencing metabolic stresses. We find, however, that the levels
144 of free ATP are unchanged after 1,6HD treatment. As a control, sodium azide (NaN_3) and 2-deoxy-
145 glucose (2DG) were used, which both depleted the cell of energy (Fig 2B). The cytosolic pH values,
146 calibrated as described in (Mouton et al. 2020), decrease mildly from 7.2 to 6,8 or 6,7 after exposure
147 to 1,6HD and 2,5HD respectively, and therefore remain in the physiological range (Fig 2C).

148 Next, we looked at the morphology and localization of different subcellular structures using GFP- or
149 RFP-tagged proteins marking the mitochondria, Golgi, peroxisome, ER, vacuole, plasma membrane,
150 nucleolus, secretory pathway, and ESCRT machinery. From visual inspection we conclude there are no
151 obvious changes in their appearance after 10 min exposure to 5% 1,6HD (Fig 2D). In contrast, the
152 appearance of microtubules and actin filaments does change after treatment with 1,6HD, which aligns
153 with some previous literature (Wheeler et al. 2016; Kroschwald, Maharana, and Simon 2017). Hsp104,
154 a disaggregase that can refold and reactivate previously aggregated proteins and responds to alcohol-
155 stress (Bösl, Grimminger, and Walter 2006; Sanchez and Lindquist 1990; Glover and Lindquist 1998;
156 Harari et al. 2022), forms foci upon exposure to 1,6HD, similar to when cells are exposed to either
157 nitrogen starvation, energy depletion or heat shock (Fig 2E), suggesting that 1,6HD induces some level
158 of protein stress. Finally, 1,6HD does not induce the formation of p-bodies (Fig 2F) or stress granules
159 (Fig 2G).

160 Taking the above together, under the conditions where mid exponentially growing cells are exposed
161 to 5% 1,6HD for 10 min, there are effects on the cytoskeleton and Hsp104 to be noted, but cell viability,
162 the pH and ATP levels in the cytosol, and the appearance of mitochondria, Golgi, peroxisomes, ER,
163 vacuoles, plasma membrane, nucleolus, the secretory and ESCRT pathways and stress granules are
164 not notably changed. While this is not an absolute proof of absence of indirect effects on nuclear

transport, the data strongly suggest that the 1,6HD-dependent effects on NPC permeability shown in Fig 1 is due to direct effects on the nuclear transport machinery. Exposure to 10 min 5% 1,6HD thus permeabilizes NPCs with surprising specificity.

1,6HD induced loss of NTRs from the NPCs disrupts the permeability barrier

Previous work proposed that the effects of 1,6HD are related to the alcohol-sensitive hydrophobic interactions between the FG-nups that maintain the permeability barrier (Patel et al. 2007; Ribbeck and Görlich 2002; Schmidt and Görlich 2015). Indeed, when the FG-domains of Nup100 (Nup100FG) in preformed condensates are exposed to the concentrations of 1,6HD that were also used in life cells (0-5%), partial solubilisation of the condensates is observed (Sup fig 1). While disruption of FG-nup interactions by 1,6HD is indeed a scenario that is supported by *in-vitro* data, it is also one that is not easy to proof or disproof in *in vivo* experiments. Alternative or additional explanations for the increased permeability of NPCs in 1,6HD treated cells that can be experimentally addressed, relate to the composition of the NPCs and to the NTRs. We explore them both.

Previous work (Shulga and Goldfarb 2003) showed that 1,6HD did not lead to release of NPC components in wild type W303 cells, but it did in a mutant lacking Nup170. We noticed that even in wild type cells the exposure to 10% 1,6HD lead to release of NPC components (data not shown). Therefore, we repeated the analysis of nup localisation, and expanded on it with an analysis of proteins levels. We assessed the effects of 5% 1,6HD on the protein levels and NPC-association of nine representative endogenously tagged nups. The five tested FG-nups (Nsp1, Nup49, Nup159, Nup100, Nup116), two of the scaffold nups (Nup133 and Nup170) and two basket nups (Nup60 and Nup2) did not show changes in expression levels by western blot (Fig 3B). Also, their localization to the nuclear envelope was unchanged, consistent with (Shulga and Goldfarb 2003) (Fig 3B). We conclude that the 10 minutes 1,6HD treatment did not lead to dissociation or degradation of the tested NPC components, and hence it is unlikely that the increased permeability is a result of changes to the Nup-composition of the NPCs.

NPCs constitute a significant amount of NTRs at any point in time and their presence critically shapes the permeability barrier (Jovanovic-Talisman et al. 2009; Kalita, Kapinos, and Lim 2021; Lowe et al. 2015; Kim et al. 2018). Therefore, we addressed the localisation and abundance of endogenously GFP-tagged NTRs after treatment with 1,6HD. The interaction between the FG-nups and NTRs are based on dynamic multivalent binding with the phenylalanine's of the FG-nups (Hoogenboom et al. 2021; Hough et al. 2015; Milles et al. 2015; Hayama et al. 2018; Sparks et al. 2018; Wing, Fung, and Chook

2022) and will thus also be sensitive to interventions disrupting hydrophobic interaction. We evaluated the localisation of endogenously GFP-tagged NTRs. Under normal conditions most NTRs are enriched at the nuclear envelope (NE) showing a punctate rim staining, e.g., Kap109, and few are enriched in the nucleus, e.g. Kap104 (Fig 4A). Strikingly, the exposure to 1,6HD led to a clear relocalisation of NTRs (Fig 4A). Kap104, Sxm1 (Kap108), Kap114, Nmd5 (Kap119), Pse1 (Kap121), Kap122 and Kap123 lose their accumulation at the NE or nucleus upon exposure to 1,6HD and distribute over the cytosol and nucleus (Fig 4A). Cse1 (Kap109), Kap120, Crm1 (Kap124) and Msn5 (Kap142) which are normally enriched at the NE, partly relocate. Kap60 and Kap95 were not visibly affected by the treatment probably related to the previously described immobile pool of Kap95 at NPCs (Lowe et al. 2015). Kap60 and Kap95 remain at NPCs while GFP-cNLS, whose active import is driven by Kap60-Kap95, loses nuclear accumulation (Fig 1B), suggesting that 1,6HD treatment increases passive permeability. When the less hydrophobic alcohol 2,5HD was used, it led to some NTRs losing their accumulation at the NE or nucleus, but always to a lesser extent compared to 1,6HD (Sup Fig 2). We conclude that the massive relocation of NTRs from NPCs may mechanistically explain the 1,6HD induced increase in the permeability of NPCs.

To further strengthen this interpretation, we sought to quantitatively correlate the concentration dependent NTR relocalisation, with the 1,6HD concentration dependent entry of the reporters used before: MG5 (Fig 1A), GFP-NLS (Fig 1B) and GFP-NES (Fig 1C). We chose Kap122 for this analysis as Kap122 clearly loses its accumulation at the NE and distributes over the cytosol and nucleus (Fig 4A). The localisation of endogenously tagged Kap122-GFP in the nucleus and NE was assessed in a strain co-expressing endogenously tagged Nup133-mCherry to mark the NE. The average nuclear accumulation of Kap122 gradually decreased from 4,3 to 3,8 to 3,1 to 2,6 to 1,6 upon exposure to zero, 0.625, 1.25, 2.5 or 5% 1,6HD. Moreover, we could correlate Kap122 relocalisation from the nuclear envelope (NE) under these conditions with the measured passive permeability of NPCs for MG5 (Fig 4C), GFP-NLS (Fig 4C) and GFP-NES (Fig 4D) with a Pearson correlation coefficient of 0.9, 0.8 and 0.9 respectively. These correlations support that 1,6HD perturbs the NPC permeability barrier by releasing the NTRs.

DISCUSSION

Here we assessed the specificity and mechanism by which 1,6-hexanediol (1,6HD), an aliphatic alcohol that interferes with hydrophobic interactions, disrupts the permeability barrier of NPCs in live baker's yeast cells. Exposure of live yeast cells to 1,6HD (10 min, 0-5%) leads to a gradual loss of the permeability barrier of NPCs. We conclude this is likely a direct effect on the nuclear transport

machinery as cell viability, the pH and ATP levels in the cytosol, and the appearance of mitochondria, Golgi, peroxisomes, ER, vacuoles, plasma membrane, nucleolus, secretory pathway and stress granules were not notably changed. There were effects on the cytoskeleton and protein homeostasis (Hsp104 foci) to be noted and we cannot exclude that 1,6 HD impacts the cell's physiology in ways that we did not monitor. Mechanistically we propose that the displacement of NTRs from the NPC underlies the loss of NPC function because 1,6HD treatment induced a massive relocation of multiple NTRs from NPCs. This displacement from the nuclear envelope quantitatively correlated with the passive permeability of NPCs.

Our studies align well with previous reports that showed that the selective properties of the FG-nups rely on the physical presence of NTRs within the NPC. The earliest study is one showing that the presence of transport factor enhances the selectivity of FG-nucleoporin-coated membranes (Jovanovic-Talisman et al. 2009). The most recent reports on detergent-permeabilized human cells show that the enrichment of NTRs at the NPCs is important for the permeability barrier by preventing passive permeability (Kalita et al. 2022). Our work adds to this by showing the importance of NTRs in live cells. The benefit being that in live cells there is a constant and large flux of transport and therefore, together with the loss of the estimated 15,6 MDa of NTRs from the central channel also 10,4 MDa worth of cargo is being lost (Kim et al. 2018). This joint loss of NTRs *and* cargo from the NPC central channel will present a major change in the macromolecular crowding and composition, and hence its physicochemical properties. How this alters the structural dynamics of the FG-nups, and if this poses a risk for NPC function would be interesting questions for the future.

Extrapolating from studies using purified FG-nup fragments that proposed that the effects of 1,6HD is related to the alcohol-sensitive hydrophobic interactions between the FG-nups (Patel et al. 2007; Ribbeck and Görlich 2002; Schmidt and Görlich 2015) one may expect that 1,6HD also alters the interactions between the FG-nups in our assays using live cells. This is, however, difficult to address in live cells. Hence it remains unclear if the NTRs are released from the NPCs as a consequence of a lowered binding affinity between FG-nups, or because 1,6HD directly lowered the binding affinity of NTRs for the FG-repeat regions. If one considers that the functional composition of central channel is a system composed of NTRs *and* FG-nups in close collaboration, then the discrimination between these scenarios becomes less important.

An unanswered question in the field is if NPCs that are dysfunctional can be detected and removed. To assess this question, one needs to be able to inducibly damage NPCs. NPC permeabilization is expected to be an intervention that triggers quality control similar to when assembly fails (Thaller et

al. 2019; Webster et al. 2016; Thaller et al. 2021). The here described method could provide a tool to study the recruitment of quality control factors and to follow the repair or degradation.

Lastly, our study may serve as a warning that the effects of 1,6HD on liquid-liquid phase separation of diverse cellular macromolecular complexes may actually be the consequence of to 1,6HD's prime effect on the NPC and cognate NTRs. We speculate that the hydrophobic and highly acidic nature of NTRs may readily compromise their stability above a critical concentration. Consistent with this is that overexpression of Sxm1, Kap95, and Kap114 is toxic to cells (Semmelink et al. 2022). In any case, a major misplacement of NTRs and associated cargo will dramatically change the nuclear and cytoplasmic proteomes and this may generally compromise their stability. The increase in the number of Hsp104 foci that we observe may indeed reflect such loss of protein homeostasis.

Altogether, this paper puts hydrophobic interactions between NTRs and FG-Nups centre stage in the explanation of the selective properties of NPCs supporting the Kap-centric model for nuclear transport proposed by the Lim laboratory (Springhower, Rosen, and Chook 2020).

MATERIAL AND METHODS

Strains and Growth conditions

All *Saccharomyces cerevisiae* strains used in this study have the BY4741 background, except yER016, which were created in the W303 background. Strains are listed in Table 2. yER016, yER020 and yER023 were created as described in (Janke et al. 2004). GFP-tagged strains were taken from the 4000-GFP yeast library (Thermofisher), RFP-tagged strains were taken from the localization database collection (Huh et al. 2003).

Cells were grown at 30˚C, with shaking at 200 RPM on Synthetic Complete (SD) medium supplemented with 2% (w/v) glucose. Cells from an overnight culture were diluted 1:10 during the day and then again for an overnight culture in SD- 2% glucose. Cells were diluted again on the day of the experiment, and grown for several hours to obtain cultures in exponential growth phase (OD_{600} 0.6-0.8) before each experiment.

Spot assay

On the day of the experiment, exponentially growing cells were treated with 5% 1,6HD or 5% 2,5HD for 10 or 30 minutes, as indicated in Fig. 2A, and diluted in sterilized milliQ water to obtain 10^6 cells/ml, and further serial diluted in milliQ water. 5µl of each dilution was spotted on YPD plates and the plates were imaged after 48H growth at 30˚C.

Microscopy

All *in vivo* experiments were performed at 30˚C. Images were acquired using a DeltaVision Elite imaging system (Cytiva) composed of an inverted microscope (IX-71; Olympus) equipped with a UPlanSApo 100x (1.4 NA) oil immersion objective, InsightSSI solid-state illumination, and an EDGE sCMOS 5.5 camera. For all experiments, stacks of 30 images with 0.2μm spacing were taken.

Protein lysate and Western Blot

20 ml of yeast culture was grown to an OD_{600} 0.8-1.2. Cells were subsequently treated with 5% 1,6HD for 10 min at 30˚C, with shaking at 200 RPM. After the treatment, cells were centrifuged, and all the following steps were performed at 4˚C. The cell lysate was resuspended in 0.25ml of lysis buffer (50mM HEPES, 200mM sodium acetate, 1mM EDTA, 5mM magnesium acetate, 5% glycerol, 1% triton x-100, 10mM β-mercaptoethanol, protease inhibitor without EDTA) and lysed in two rounds of bead-beating in a Fastprep device (MP biomedicals). Lysates were cleared by consecutive centrifugations at 6000 x g for 5 min, followed by centrifugation of the supernatant at 17700 x g for 5 min. The resulting supernatant was centrifuged once more at 17700 x g.

Western blots were performed as follows: whole cell lysates were separated by SDS-PAGE. The proteins were subsequently transferred to PVDF membranes. After blocking with 5% skim milk in TBS-T, GFP-tagged proteins were detected with anti-GFP (Santa Cruz sc-9996 HRP) was used, followed by HRP-conjugated mouse IgG kappa binding protein (Santa Cruz sc-516102, m-igGκ BP-HRP).

Expression and purification of nucleoporin FG-domains

Nup100FG domains were expressed and purified as described in (Kuiper et al. 2022). In short: FG-domains proteins with an N terminal His-tag and a unique C-terminal cysteine were expressed in *Escherichia coli*, by induction with 0.5mM IPTG and purified from cell extracts on a Nickel-Sepharose column under denaturing conditions (2M GuHCl, 100mM Tris-HCl pH 8). The C-terminal cysteine was reduced with DTT and blocked by modification with Iodoacetamide. Protein purity was checked with SDS-PAGE and subsequent Brilliant Blue staining.

Spin Assay

A concentrated stock of 100μM Nup100FG domains in 2M GuHCl, 100mM Tris-HCl pH 8, was diluted to 3μM into TBS (50mM Tris-HCl, 150mM NaCl pH 8). The protein was left to self-assemble into particles for 1h at RT, and then the protein was treated for 10 min with different concentrations of 1,6HD. Samples were centrifuged (17.700 x g for 10 min at RT), and soluble and insoluble fractions were run separately on SDS PAA gels. Gels were stained with Brilliant Blue G (Sigma-Aldrich, G-250)

and imaged using a BioRad chemidoc (BioRad). Band intensities were determined using Fiji (Image J, National Institute of Health).

Determining the intracellular pH with the pHluorin sensor

pHluorin ratios were calibrated in live cells in buffers with a pH of 5, 5.5, 6, 6.5, 7, 7.5, and 8, as described in (Mouton et al. 2020). The FRET/CFP and FRET/mEGFP (F390/F475) ratios were determined from cells on a glass slide. Cells were then treated with 1,6HD as described in Fig 2, and a calibration curve was used to determine the pH change after treatment.

ATP sensor values and free ATP levels

Cells expressing a FRET-based ATP sensor (Semmelink et al. 2022), were used to determine free ATP levels as described in (Semmelink et al. 2022). Cells were treated as described in Fig 2, imaged, and the FRET over GFP ratio was calculated using Fiji (see below).

Image Analysis

All images were processed using Fiji (Image J, National Institute of Health). For each image, the z-stack with the best focus was selected. For GFP-tagged reporters, we determined the fluorescence around the nuclear envelope and subtracted the background from outside the cell. For pHluorin and the ATP sensor, we determined the fluorescence in each channel for each cell and took the fluorescence of the entire cell and subtracted the background from a region outside the cell for each channel. The respective ratios were subsequently calculated. To quantify the nuclear localization (N/C ratio) of the GFP-based reporters and Kap122, the average fluorescent intensity of the nucleus and the cytosol was measured. The nucleus area was determined using either the mCherry-TM reporter (pACM063) that indicated the nuclear envelope (Fig 1) or Nup133-mCherry (Fig 4B). A section of the cytosol excluding the vacuole was selected to measure the fluorescence in the cytosol.

Statistical Analysis

Statistical parameters, including the number of cells analyzed, are reported in figure legends. All regressions and correlations leading to the sigmoidal curve equation, R^2, and all Pearson's correlation statistics were done in GraphPad Prism.

ACKNOWLEDGEMENTS

ERB and TO are supported by PhD-fellowships from the Graduate School of Medical Sciences of the University of Groningen. ERB, AS, LMV, are supported by a Vici grant (VI.C.192.031) from the

354 Netherlands Organisation for Scientific Research. We want to thank Amarins Blaauwbroek for practical
355 assistance.

356 **AUTHOR CONTRIBUTIONS**

357 ERB and LMV conceived the project. ERB designed, performed and analysed all experiments with help
358 from SNM (Fig. 2BC) and TO (Supfig1). The manuscript was written by ERB and LMV with input of all
359 authors.

360

361 **COMPETING INTERESTS**

362 The authors declare no competing interests.

363

364 **DATA AND REAGENT AVAILABILITY**

365 All data and reagents are available upon request.

366

367 **REFERENCES**

368 Ader, Christian, Steffen Frey, Werner Maas, Hermann Broder Schmidt, Dirk Görlich, and Marc Baldus.
369 2010. “Amyloid-like Interactions within Nucleoporin FG Hydrogels.” *Proceedings of the National*
370 *Academy of Sciences of the United States of America* 107 (14): 6281–85.
371 https://doi.org/10.1073/pnas.0910163107.

372 Bayliss, Richard, Trevor Littlewood, and Murray Stewart. 2000. “Structural Basis for the Interaction
373 between FxFG Nucleoporin Repeats and Importin-β in Nuclear Trafficking.” *Cell* 102 (1): 99–
374 108. https://doi.org/10.1016/S0092-8674(00)00014-3.

375 Bösl, Benjamin, Valerie Grimminger, and Stefan Walter. 2006. “The Molecular Chaperone Hsp104-A
376 Molecular Machine for Protein Disaggregation.” *Journal of Structural Biology* 156 (1): 139–48.
377 https://doi.org/10.1016/j.jsb.2006.02.004.

378 Celetti, Giorgia, Giulia Paci, Joana Caria, Virginia VanDelinder, George Bachand, and Edward A.
379 Lemke. 2020. “The Liquid State of FG-Nucleoporins Mimics Permeability Barrier Properties of
380 Nuclear Pore Complexes.” *Journal of Cell Biology* 219 (1).
381 https://doi.org/10.1083/jcb.201907157.

382 Chowdhury, Rajdeep, Abhishek Sau, and Siegfried M. Musser. 2022. “Super-Resolved 3D Tracking of

383 Cargo Transport through Nuclear Pore Complexes." *Nature Cell Biology* 24 (1): 112–22.
384 https://doi.org/10.1038/s41556-021-00815-6.

385 Davis, Luke K., Ian J. Ford, and Bart W. Hoogenboom. 2022. "Crowding-Induced Phase Separation of
386 Nuclear Transport Receptors in FG Nucleoporin Assemblies." *ELife* 11: 1–20.
387 https://doi.org/10.7554/eLife.72627.

388 Dultz, Elisa, Matthias Wojtynek, Ohad Medalia, and Evgeny Onischenko. 2022. "The Nuclear Pore
389 Complex: Birth, Life, and Death of a Cellular Behemoth." *Cells* 11 (9): 1–28.
390 https://doi.org/10.3390/cells11091456.

391 Fernandez-Martinez, Javier, and Michael P. Rout. 2021. "One Ring to Rule Them All? Structural and
392 Functional Diversity in the Nuclear Pore Complex." *Trends in Biochemical Sciences* 46 (7): 595–
393 607. https://doi.org/10.1016/j.tibs.2021.01.003.

394 Fisher, Patrick D.Ellis, Qi Shen, Bernice Akpinar, Luke K. Davis, Kenny Kwok Hin Chung, David
395 Baddeley, Andela Šarić, et al. 2018. "A Programmable DNA Origami Platform for Organizing
396 Intrinsically Disordered Nucleoporins within Nanopore Confinement." *ACS Nano* 12 (2): 1508–
397 18. https://doi.org/10.1021/acsnano.7b08044.

398 Fragasso, Alessio, Hendrik W de Vries, John Andersson, Eli O van der Sluis, Erik van der Giessen,
399 Patrick R Onck, and Cees Dekker. 2022. "Transport Receptor Occupancy in Nuclear Pore
400 Complex Mimics." *Nano Research* 15 (11): 9689–9703.

401 Frey, Steffen, Ralf P. Richter, and Dirk Görlich. 2006. "FG-Rich Repeats of Nuclear Pore Proteins Form
402 a Three-Dimensional Meshwork with Hydrogel-like Properties." *Science* 314 (5800): 815–17.
403 https://doi.org/10.1126/science.1132516.

404 Ghavami, Ali, Liesbeth M. Veenhoff, Erik Van Der Giessen, and Patrick R. Onck. 2014. "Probing the
405 Disordered Domain of the Nuclear Pore Complex through Coarse-Grained Molecular Dynamics
406 Simulations." *Biophysical Journal* 107 (6): 1393–1402.
407 https://doi.org/10.1016/j.bpj.2014.07.060.

408 Glover, John R., and Susan Lindquist. 1998. "Hsp104, Hsp70, and Hsp40: A Novel Chaperone System
409 That Rescues Previously Aggregated Proteins." *Cell* 94 (1): 73–82.
410 https://doi.org/10.1016/S0092-8674(00)81223-4.

411 Hampoelz, Bernhard, Amparo Andres-Pons, Panagiotis Kastritis, and Martin Beck. 2019. "Structure
412 and Assembly of the Nuclear Pore Complex." *Annual Review of Biophysics* 48: 515–36.
413 https://doi.org/10.1146/annurev-biophys-052118-115308.

414 Harari, Anna, Guy Zoltsman, Tal Levin, and Rina Rosenzweig. 2022. “Hsp104 N-Terminal Domain
415 Interaction with Substrates Plays a Regulatory Role in Protein Disaggregation.” *FEBS Journal*
416 289 (17): 5359–77. https://doi.org/10.1111/febs.16441.

417 Hayama, Ryo, Samuel Sparks, Lee M. Hecht, Kaushik Dutta, Jerome M. Karp, Christina M. Cabana,
418 Michael P. Rout, David Cowburn, and Norma M. Allewell. 2018. “Thermodynamic
419 Characterization of the Multivalent Interactions Underlying Rapid and Selective Translocation
420 through the Nuclear Pore Complex.” *Journal of Biological Chemistry* 293 (12): 4555–63.
421 https://doi.org/10.1074/jbc.AC117.001649.

422 Hoogenboom, Bart W., Loren E. Hough, Edward A. Lemke, Roderick Y.H. Lim, Patrick R. Onck, and
423 Anton Zilman. 2021. “Physics of the Nuclear Pore Complex: Theory, Modeling and Experiment.”
424 *Physics Reports* 921: 1–53. https://doi.org/10.1016/j.physrep.2021.03.003.

425 Hough, Loren E., Kaushik Dutta, Samuel Sparks, Deniz B. Temel, Alia Kamal, Jaclyn Tetenbaum-
426 Novatt, Michael P. Rout, and David Cowburn. 2015. “The Molecular Mechanism of Nuclear
427 Transport Revealed by Atomic-Scale Measurements.” *ELife* 4 (September): 1–23.
428 https://doi.org/10.7554/eLife.10027.

429 Huang, Kai, and Igal Szleifer. 2020. “Modeling the Nucleoporins That Form the Hairy Pores.”
430 *Biochemical Society Transactions* 48 (4): 1447–61. https://doi.org/10.1042/BST20190941.

431 Huh, W K., Falvo, J V., Gerke, L C., Carroll, et al. 2003. “Global Analysis of Protein Localization in
432 Budding Yeast.” *Nature* 425 (6959): 686–91. http://yeastgfp.ucsf.edu.

433 Imamura, Hiromi, Kim P. Huynh Nhat, Hiroko Togawa, Kenta Saito, Ryota Iino, Yasuyuki Kato-
434 Yamada, Takeharu Nagai, and Hiroyuki Noji. 2009. “Visualization of ATP Levels inside Single
435 Living Cells with Fluorescence Resonance Energy Transfer-Based Genetically Encoded
436 Indicators.” *Proceedings of the National Academy of Sciences* 106 (37): 15651–56.
437 https://doi.org/10.1073/pnas.0904764106.

438 Isgro, Timothy A., and Klaus Schulten. 2007. “Association of Nuclear Pore FG-Repeat Domains to
439 NTF2 Import and Export Complexes.” *Journal of Molecular Biology* 366 (1): 330–45.
440 https://doi.org/10.1016/j.jmb.2006.11.048.

441 Jäggi, Rainer D., Alfredo Franco-Obregón, Petra Mühlhäusser, Franziska Thomas, Ulrike Kutay, and
442 Klaus Ensslin. 2003. “Modulation of Nuclear Pore Topology by Transport Modifiers.” *Biophysical*
443 *Journal* 84 (1): 665–70. https://doi.org/10.1016/S0006-3495(03)74886-3.

444 Janke, Carsten, Maria M. Magiera, Nicole Rathfelder, Christof Taxis, Simone Reber, Hiromi Maekawa,

Alexandra Moreno-Borchart, et al. 2004. “A Versatile Toolbox for PCR-Based Tagging of Yeast Genes: New Fluorescent Proteins, More Markers and Promoter Substitution Cassettes.” *Yeast* 21 (11): 947–62. https://doi.org/10.1002/yea.1142.

Jovanovic-Talisman, Tijana, Jaclyn Tetenbaum-Novatt, Anna Sophia McKenney, Anton Zilman, Reiner Peters, Michael P. Rout, and Brian T. Chait. 2009. “Artificial Nanopores That Mimic the Transport Selectivity of the Nuclear Pore Complex.” *Nature* 457 (7232): 1023–27. https://doi.org/10.1038/nature07600.

Kalita, Joanna, Larisa E. Kapinos, and Roderick Y.H. Lim. 2021. “On the Asymmetric Partitioning of Nucleocytoplasmic Transport – Recent Insights and Open Questions.” *Journal of Cell Science* 134 (7). https://doi.org/10.1242/jcs.240382.

Kalita, Joanna, Larisa E. Kapinos, Tiantian Zheng, Chantal Rencurel, Anton Zilman, and Roderick Y.H. Lim. 2022. “Karyopherin Enrichment and Compensation Fortifies the Nuclear Pore Complex against Nucleocytoplasmic Leakage.” *Journal of Cell Biology* 221 (3). https://doi.org/10.1083/jcb.202108107.

Kapinos, Larisa E., Binlu Huang, Chantal Rencurel, and Roderick Y.H. Lim. 2017. “Karyopherins Regulate Nuclear Pore Complex Barrier and Transport Function.” *Journal of Cell Biology* 216 (11): 3609–24. https://doi.org/10.1083/jcb.201702092.

Kapinos, Larisa E., Rafael L. Schoch, Raphael S. Wagner, Kai D. Schleicher, and Roderick Y.H. Lim. 2014. “Karyopherin-Centric Control of Nuclear Pores Based on Molecular Occupancy and Kinetic Analysis of Multivalent Binding with FG Nucleoporins.” *Biophysical Journal* 106 (8): 1751–62. https://doi.org/10.1016/j.bpj.2014.02.021.

Kim, Seung Joong, Javier Fernandez-Martinez, Ilona Nudelman, Yi Shi, Wenzhu Zhang, Barak Raveh, Thurston Herricks, et al. 2018. “Integrative Structure and Functional Anatomy of a Nuclear Pore Complex.” *Nature* 555 (7697): 475–82. https://doi.org/10.1038/nature26003.

Kowalczyk, Stefan W., Larisa Kapinos, Timothy R. Blosser, Tomás Magalhães, Pauline Van Nies, Roderick Y.H. Lim, and Cees Dekker. 2011. “Single-Molecule Transport across an Individual Biomimetic Nuclear Pore Complex.” *Nature Nanotechnology* 6 (7): 433–38. https://doi.org/10.1038/nnano.2011.88.

Kroschwald, Sonja, Shovamayee Maharana, and Alberti Simon. 2017. “Hexanediol: A Chemical Probe to Investigate the Material Properties of Membrane-Less Compartments.” *Matters*, 1–7. https://doi.org/10.19185/matters.201702000010.

476 Kuiper, E. F.Elsiena, Paola Gallardo, Tessa Bergsma, Muriel Mari, Maiara Kolbe Musskopf, Jeroen
477 Kuipers, Ben N.G. Giepmans, et al. 2022. “The Chaperone DNAJB6 Surveils FG-Nucleoporins and
478 Is Required for Interphase Nuclear Pore Complex Biogenesis.” *Nature Cell Biology* 24 (11):
479 1584–94. https://doi.org/10.1038/s41556-022-01010-x.

480 Lin, Yi, Eiichiro Mori, Masato Kato, Siheng Xiang, Leeju Wu, Ilmin Kwon, and Steven L. McKnight.
481 2016. “Toxic PR Poly-Dipeptides Encoded by the C9orf72 Repeat Expansion Target LC Domain
482 Polymers.” *Cell* 167 (3): 789-802.e12. https://doi.org/10.1016/j.cell.2016.10.003.

483 Lindt, Joris Van, Tamas Lazar, Donya Pakravan, Manon Demulder, Attila Meszaros, Ludo Van Den
484 Bosch, Dominique Maes, and Peter Tompa. 2022. “F/YGG-Motif Is an Intrinsically Disordered
485 Nucleic-Acid Binding Motif.” *RNA Biology* 19 (1): 622–35.
486 https://doi.org/10.1080/15476286.2022.2066336.

487 Lowe, Alan R., Jeffrey H. Tang, Jaime Yassif, Michael Graf, William Y.C. Huang, Jay T. Groves, Karsten
488 Weis, and Jan T. Liphardt. 2015. “Importin-β Modulates the Permeability of the Nuclear Pore
489 Complex in a Ran-Dependent Manner.” *ELife* 2015 (4): 1–24.
490 https://doi.org/10.7554/eLife.04052.

491 Mattheyses, Alexa L., Martin Kampmann, Claire E. Atkinson, and Sanford M. Simon. 2010.
492 “Fluorescence Anisotropy Reveals Order and Disorder of Protein Domains in the Nuclear Pore
493 Complex.” *Biophysical Journal* 99 (6): 1706–17. https://doi.org/10.1016/j.bpj.2010.06.075.

494 Meinema, Anne C., Bert Poolman, and Liesbeth M. Veenhoff. 2013. “Quantitative Analysis of
495 Membrane Protein Transport Across the Nuclear Pore Complex.” *Traffic* 14 (5): 487–501.
496 https://doi.org/10.1111/tra.12048.

497 Miesenböck, Gero, Dino A De Angelis, and James E Rothman. 1998. “Visualizing Secretion and
498 Synaptic Transmission with PH-Sensitive Green Fluorescent Proteins.” *Nature* 394 (July): 192–
499 95. https://www.nature.com/articles/BF28190.

500 Milles, Sigrid, Davide Mercadante, Iker Valle Aramburu, Malene Ringkjøbing Jensen, Niccolò
501 Banterle, Christine Koehler, Swati Tyagi, et al. 2015. “Plasticity of an Ultrafast Interaction
502 between Nucleoporins and Nuclear Transport Receptors.” *Cell* 163 (3): 734–45.
503 https://doi.org/10.1016/j.cell.2015.09.047.

504 Molliex, Amandine, Jamshid Temirov, Jihun Lee, Maura Coughlin, Anderson P. Kanagaraj, Hong Joo
505 Kim, Tanja Mittag, and J. Paul Taylor. 2015. “Phase Separation by Low Complexity Domains
506 Promotes Stress Granule Assembly and Drives Pathological Fibrillization.” *Cell* 163 (1): 123–33.

https://doi.org/10.1016/j.cell.2015.09.015.

Mouton, Sara N., David J. Thaller, Matthew M. Crane, Irina L. Rempel, Owen Terpstra, Anton Steen, Matt Kaeberlein, C. Patrick Lusk, Arnold J. Boersma, and Liesbeth M. Veenhoff. 2020. "A Physicochemical Perspective of Aging from Single-Cell Analysis of Ph, Macromolecular and Organellar Crowding in Yeast." *ELife* 9: 1–42. https://doi.org/10.7554/ELIFE.54707.

Onischenko, Evgeny, Jeffrey H. Tang, Kasper R. Andersen, Kevin E. Knockenhauer, Pascal Vallotton, Carina P. Derrer, Annemarie Kralt, et al. 2017. "Natively Unfolded FG Repeats Stabilize the Structure of the Nuclear Pore Complex." *Cell* 171 (4): 904-917.e19. https://doi.org/10.1016/j.cell.2017.09.033.

Paci, Giulia, Joana Caria, and Edward A. Lemke. 2021. "Cargo Transport through the Nuclear Pore Complex at a Glance." *Journal of Cell Science* 134 (2). https://doi.org/10.1242/jcs.247874.

Patel, Samir S., Brian J. Belmont, Joshua M. Sante, and Michael F. Rexach. 2007. "Natively Unfolded Nucleoporins Gate Protein Diffusion across the Nuclear Pore Complex." *Cell* 129 (1): 83–96. https://doi.org/10.1016/j.cell.2007.01.044.

Popken, Petra, Ali Ghavami, Patrick R. Onck, Bert Poolman, and Liesbeth M. Veenhoff. 2015. "Size-Dependent Leak of Soluble and Membrane Proteins through the Yeast Nuclear Pore Complex." *Molecular Biology of the Cell* 26 (7): 1386–94. https://doi.org/10.1091/mbc.E14-07-1175.

Rempel, Irina L., Matthew M. Crane, David J Thaller, Ankur Mishra, Daniel P.M. Jansen, Georges Janssens, Petra Popken, et al. 2019. "Age-Dependent Deterioration of Nuclear Pore Assembly in Mitotic Cells Decreases Transport Dynamics." *ELife* 8 (June): 1–26. https://doi.org/10.7554/eLife.48186.

Ribbeck, Katharina, and Dirk Görlich. 2002. "The Permeability Barrier of Nuclear Pore Complexes Appears to Operate via Hydrophobic Exclusion." *EMBO Journal* 21 (11): 2664–71. https://doi.org/10.1093/emboj/21.11.2664.

Sakiyama, Yusuke, Adam Mazur, Larisa E. Kapinos, and Roderick Y.H. Lim. 2016. "Spatiotemporal Dynamics of the Nuclear Pore Complex Transport Barrier Resolved by High-Speed Atomic Force Microscopy." *Nature Nanotechnology* 11 (8): 719–23. https://doi.org/10.1038/nnano.2016.62.

Sanchez, Yolanda, and Susan L. Lindquist. 1990. "HSP104 Required for Induced Thermotolerance." *Science* 248 (4959): 1112–15. https://doi.org/10.1126/science.2188365.

Schindelin, Johannes, Ignacio Arganda-Carreras, Erwin Frise, Verena Kaynig, Mark Longair, Tobias Pietzsch, Stephan Preibisch, et al. 2012. "Fiji: An Open-Source Platform for Biological-Image

538 Analysis." *Nature Methods* 9 (7): 676–82. https://doi.org/10.1038/nmeth.2019.

539 Schmidt, Hermann B.roder, and Dirk Görlich. 2015. "Nup98 FG Domains from Diverse Species
540 Spontaneously Phase-Separate into Particles with Nuclear Pore-like Permselectivity." *ELife* 4: 1–
541 30. https://doi.org/10.7554/eLife.04251.

542 Schnell, Steven J, Mark Tingey, and Weidong Yang. 2022. "Speed Microscopy: High-Speed Single
543 Molecule Tracking and Mapping of Nucleocytoplasmic Transport." *Methods Mol Biol* 2502:
544 353–71. https://doi.org/https://doi.org/10.1007/978-1-0716-2337-4_23.

545 Semmelink, Marije F W, Hamidreza Jafarinia, Justina C Wolters, Teodora Gheorghe, Sara N Mouton,
546 Patrick R Onck, Liesbeth M Veenhoff, Nuclear Pore Complex, and Nuclear Transport Receptor.
547 2022. "Nuclear Transport under Stress Phenocopies Transport Defects in Models of C9Orf72
548 ALS," 1–38. bioRxiv 2022.04.13.488135; doi: https://doi.org/10.1101/2022.04.13.488135

549 Shi, Kevin Y., Eiichiro Mori, Zehra F. Nizami, Yi Lin, Masato Kato, Siheng Xiang, Leeju C. Wu, et al.
550 2017. "Toxic PRn Poly-Dipeptides Encoded by the C9orf72 Repeat Expansion Block Nuclear
551 Import and Export." *Proceedings of the National Academy of Sciences of the United States of*
552 *America* 114 (7): E1111–17. https://doi.org/10.1073/pnas.1620293114.

553 Shulga, Nataliya, and David S. Goldfarb. 2003. "Binding Dynamics of Structural Nucleoporins Govern
554 Nuclear Pore Complex Permeability and May Mediate Channel Gating." *Molecular and Cellular*
555 *Biology* 23 (2): 534–42. https://doi.org/10.1128/mcb.23.2.534-542.2003.

556 Sparks, Samuel, Deniz B. Temel, Michael P. Rout, and David Cowburn. 2018. "Deciphering the 'Fuzzy'
557 Interaction of FG Nucleoporins and Transport Factors Using Small-Angle Neutron Scattering."
558 *Structure* 26 (3): 477-484.e4. https://doi.org/10.1016/j.str.2018.01.010.

559 Springhower, Charis E., Michael K. Rosen, and Yuh Min Chook. 2020. "Karyopherins and
560 Condensates." *Current Opinion in Cell Biology* 64: 112–23.
561 https://doi.org/10.1016/j.ceb.2020.04.003.

562 Thaller, David J., Matteo Allegretti, Sapan Borah, Paolo Ronchi, Martin Beck, and C. Patrick Lusk.
563 2019. "An Escrt-Lem Protein Surveillance System Is Poised to Directly Monitor the Nuclear
564 Envelope and Nuclear Transport System." *ELife* 8: 1–36. https://doi.org/10.7554/eLife.45284.

565 Thaller, David J., Danqing Tong, Christopher J. Marklew, Nicholas R. Ader, Philip J. Mannino, Sapan
566 Borah, Megan C. King, Barbara Ciani, and C. Patrick Lusk. 2021. "Direct Binding of ESCRT Protein
567 Chm7 to Phosphatidic Acid-Rich Membranes at Nuclear Envelope Herniations." *Journal of Cell*
568 *Biology* 220 (3). https://doi.org/10.1083/JCB.202004222.

569 Timney, Benjamin L., Barak Raveh, Roxana Mironska, Jill M. Trivedi, Seung Joong Kim, Daniel Russel,
570 Susan R. Wente, Andrej Sali, and Michael P. Rout. 2016. “Simple Rules for Passive Diffusion
571 through the Nuclear Pore Complex.” *Journal of Cell Biology* 215 (1): 57–76.
572 https://doi.org/10.1083/jcb.201601004.

573 Webster, Brant M, David J Thaller, Jens Jäger, Sarah E Ochmann, Sapan Borah, and C Patrick Lusk.
574 2016. “Chm7 and Heh1 Collaborate to Link Nuclear Pore Complex Quality Control with Nuclear
575 Envelope Sealing.” *The EMBO Journal* 35 (22): 2447–67.
576 https://doi.org/10.15252/embj.201694574.

577 Wheeler, Joshua R., Tyler Matheny, Saumya Jain, Robert Abrisch, and Roy Parker. 2016. “Distinct
578 Stages in Stress Granule Assembly and Disassembly.” *ELife* 5 (Se): 1–25.
579 https://doi.org/10.7554/eLife.18413.

580 Wing, Casey E., Ho Yee Joyce Fung, and Yuh Min Chook. 2022. “Karyopherin-Mediated
581 Nucleocytoplasmic Transport.” *Nature Reviews Molecular Cell Biology* 23 (5): 307–28.
582 https://doi.org/10.1038/s41580-021-00446-7.

583 Yu, M, M Heidari, S Mikhaleva, P S Tan, S Mingu, H Ruan, C D Reinkermeier, et al. 2022. “Deciphering
584 the Conformations and Dynamics of FG-Nucleoporins <Em>in Situ</Em>” *BioRxiv*,
585 2022.07.07.499201. http://biorxiv.org/content/early/2022/07/08/2022.07.07.499201.abstract.

586 Zheng, Tiantian, and Anton Zilman. 2023. “Self-Regulation of the Nuclear Pore Complex Enables
587 Clogging-Free Crowded Transport.” *PNAS* 120 (7). https://doi.org/10.1073/pnas.2212874120/-
588 /DCSupplemental.Published.

589

590 **FIGURES**

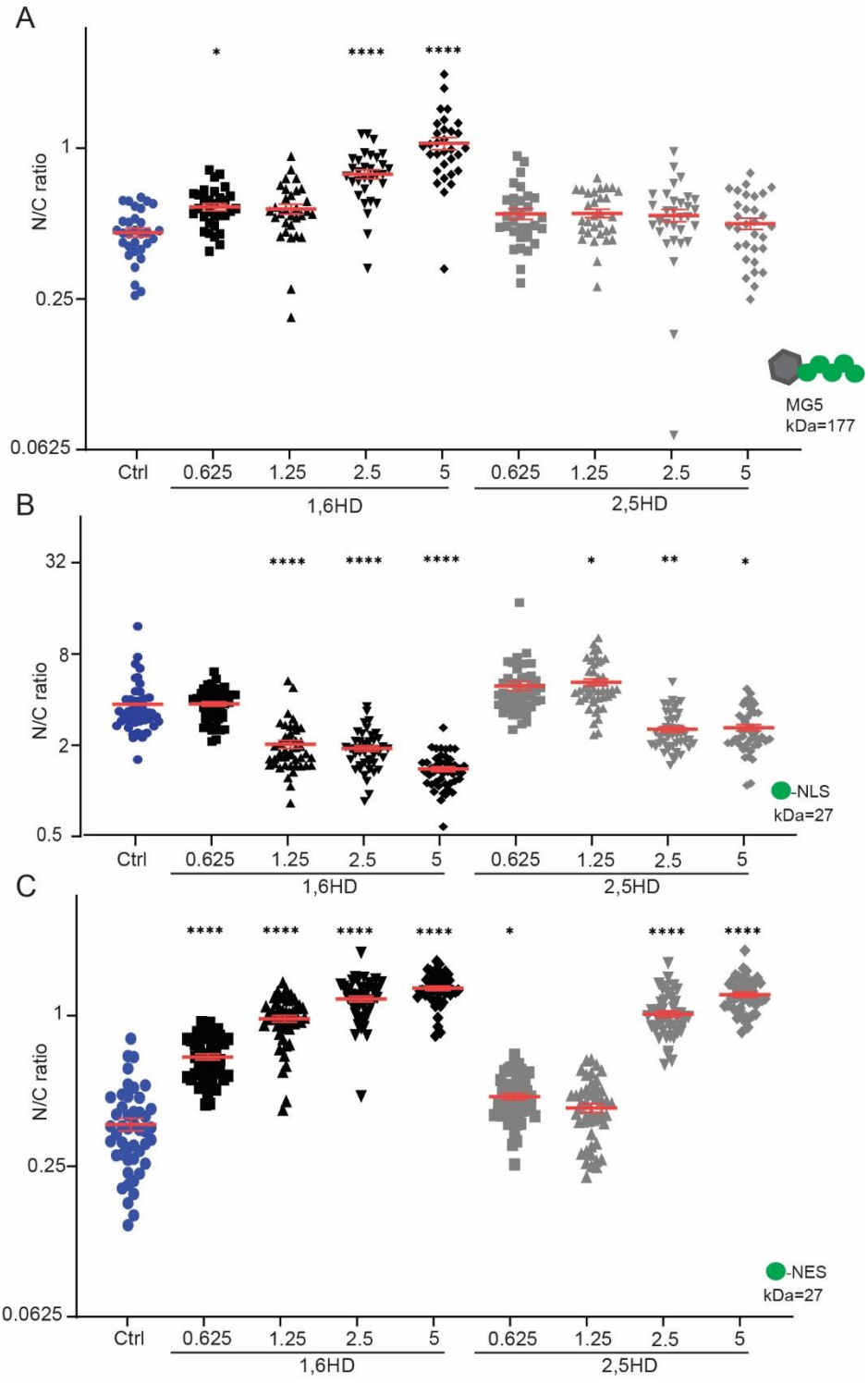

591

592 **Figure 1: Disruption of NPC permeability barrier by 1,6HD.** (A-C) Nuclear compartmentalization of
593 GFP-based reporter proteins (MG5, GFP-NES, GFP-NLS) in yeast cells exposed for 10 min with the
594 indicated concentrations of 1,6HD or 2,5HD. MG5 is a fusion of Maltose Binding Protein and 5 GFPs;
595 GFP-NLS features the classical Simian Virus 40 NLS and GFP-NES the Stress-Seventy subfamily B1 NES.
596 The N/C ratio is the ratio of the average fluorescence in the nucleus (N) over that in the cytoplasm (C).

One-way ANOVA with Dunnett's multiple comparison test comparing treatment to control was used to calculate the statistical significance of (A) MG5 and (C) GFP-NES, while the non-parametrical Kruskal-Wallis with Dunn's multiple comparison test comparing treatment to control was used to calculate the statistical significance of (B) GFP-NLS. Error bars reflect SEM from the mean of three independent experiments. At least 30 cells per condition were analysed. P-values*<0,05 **<0,01 ****<0,0001.

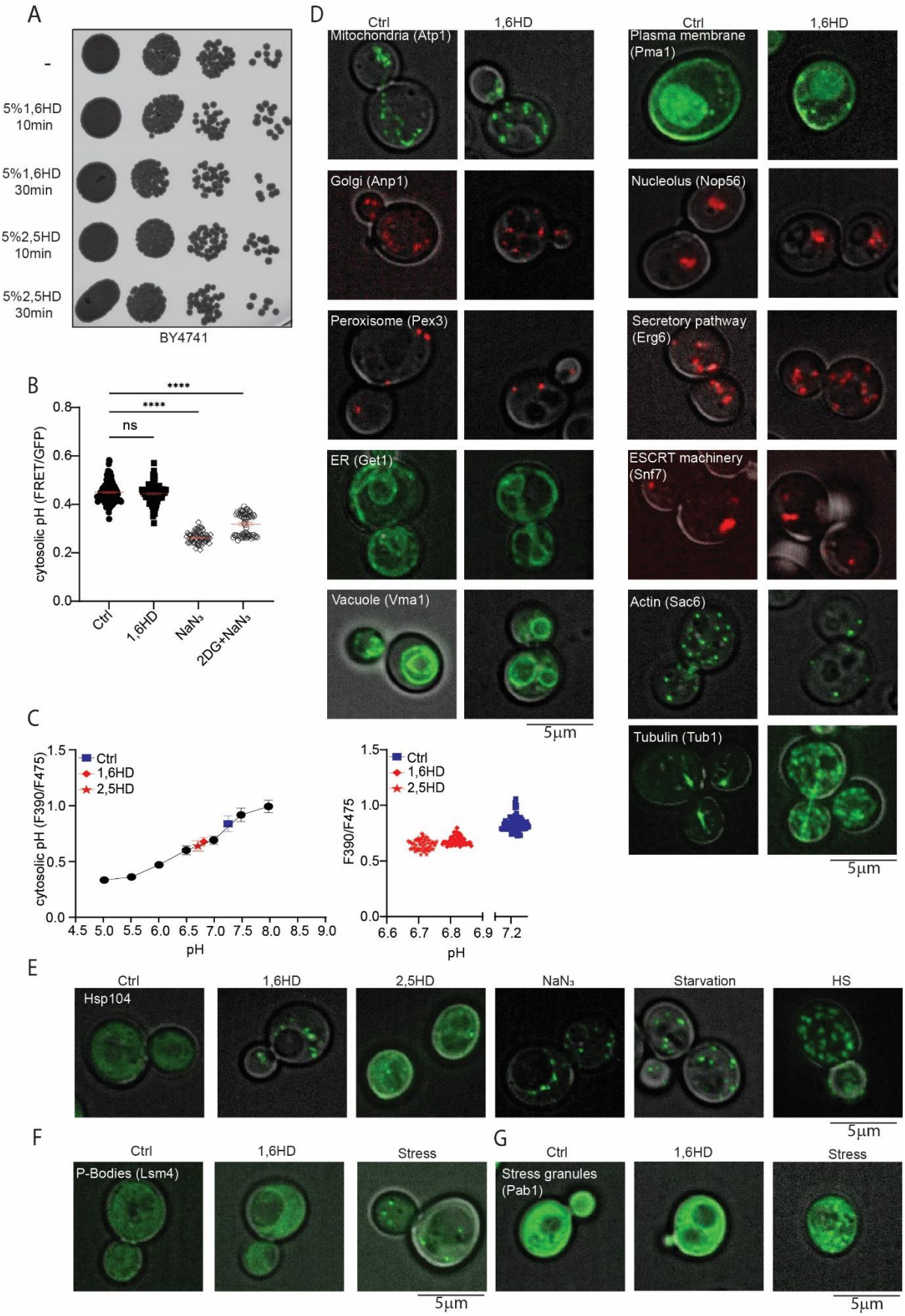

603

Figure 2: Impact of 1,6HD on cell survival, physiology and subcellular structures. (A) Growth assay showing serial dilutions of cultures exposed to 5% 1,6HD or 2,5HD for the indicated times. (B) Free ATP levels in cells measured using a FRET-based ATP-sensor; lower FRET/GFP ratio indicates lower free ATP. Cells were untreated (ctrl), exposed to 5% 1,6HD for 10 min, or exposed for 30 min to metabolic poisons azide (NaN_3) or to NaN_3 plus deoxyglucose (NaN_3 + 2DG). The error bar of the scatter plot reflects SEM from the mean of three independent experiments. At least 60 cells per condition were analysed. Non parametric Mann-Whitney test was used to calculate statistical significance in FRET/GFP ratios comparing treatment to control. (C) Calibration curve for cytosolic pH values of the pH sensor pHluorin (F390/F475) in cells (black circles). The pH before (ctrl, blue squares) and after 10 min exposure to 1,6HD (red diamonds) or 2,5 HD (red stars) are indicated. Each point represents data from 60 cells (left grapgh), individual measurements are shown (right graph). (D) Fluorescence images of different cellular structures endogenously tagged with either GFP or mCherry, before and after 10 min exposure to 5% 1,6HD. (E) Fluorescence images showing localization of endogenously tagged Hsp104-GFP after 10 min exposure to 5% 1,6HD or 5% 2,5HD and under indicated stress conditions. (F,G) Fluorescence images showing localization of endogenously tagged Lsm4 (P-bodies, F) or Pab1 (Stress granules, G) with GFP after 10 min exposure with 5% 1,6HD and after induction of stress. Representative images of three independent replicates. The scales bars are 5μm.

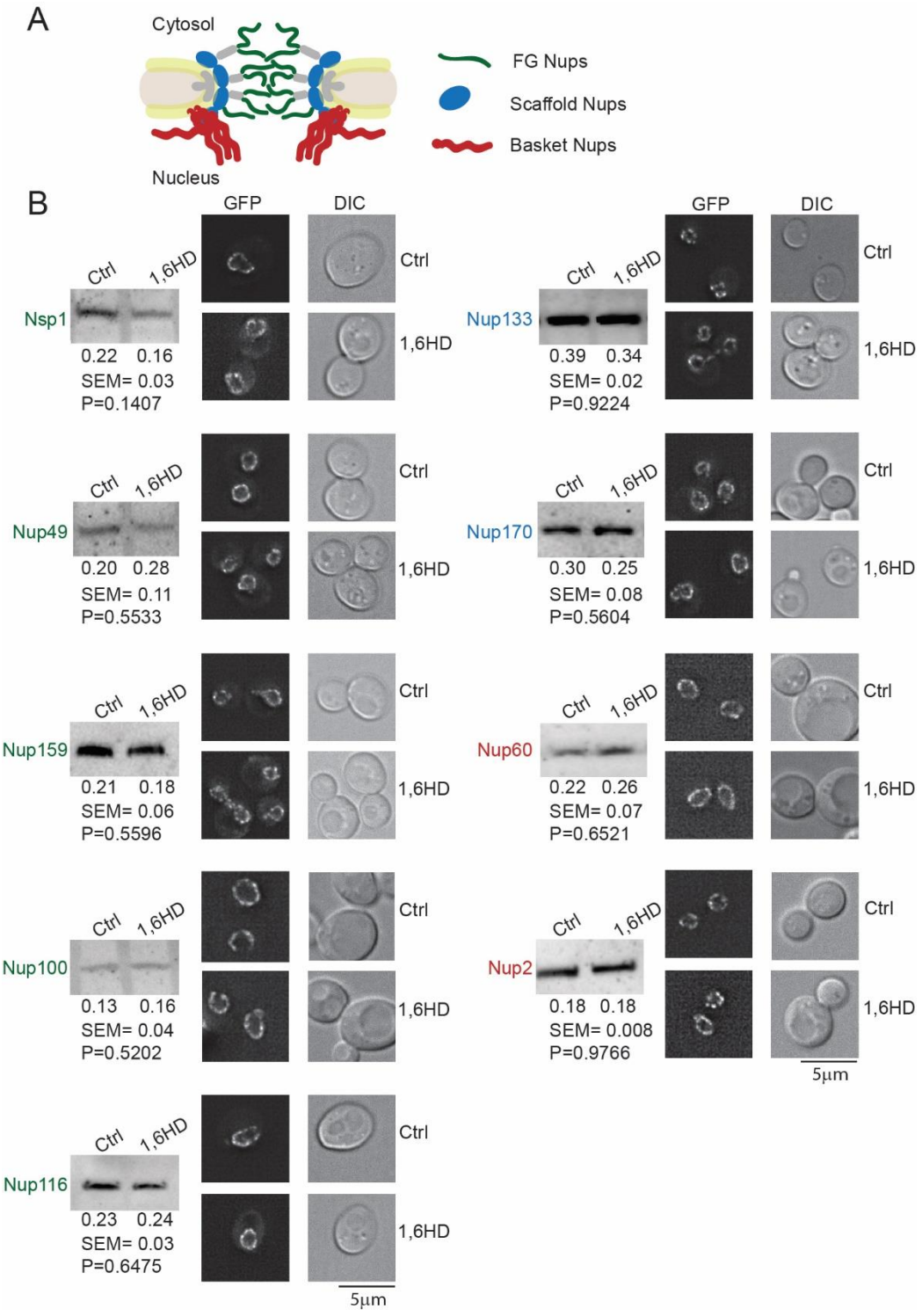

Figure 3: Impact of 1,6HD on the abundance and localization of NPC components. (A) Cartoon representation of NPC indicating the position of the nups analyzed in B. (B) Western blot of endogenous Nup-GFP protein levels before and after 10 min exposure to 5% 1,6HD; quantification gives mean, SEM and P values from at least three independent replicates. Fluorescence images of endogenously GFP-tagged nups after 10 min exposure with 5% 1,6HD. Representative images of three independent replicates. The scale bar is 5µm.

628

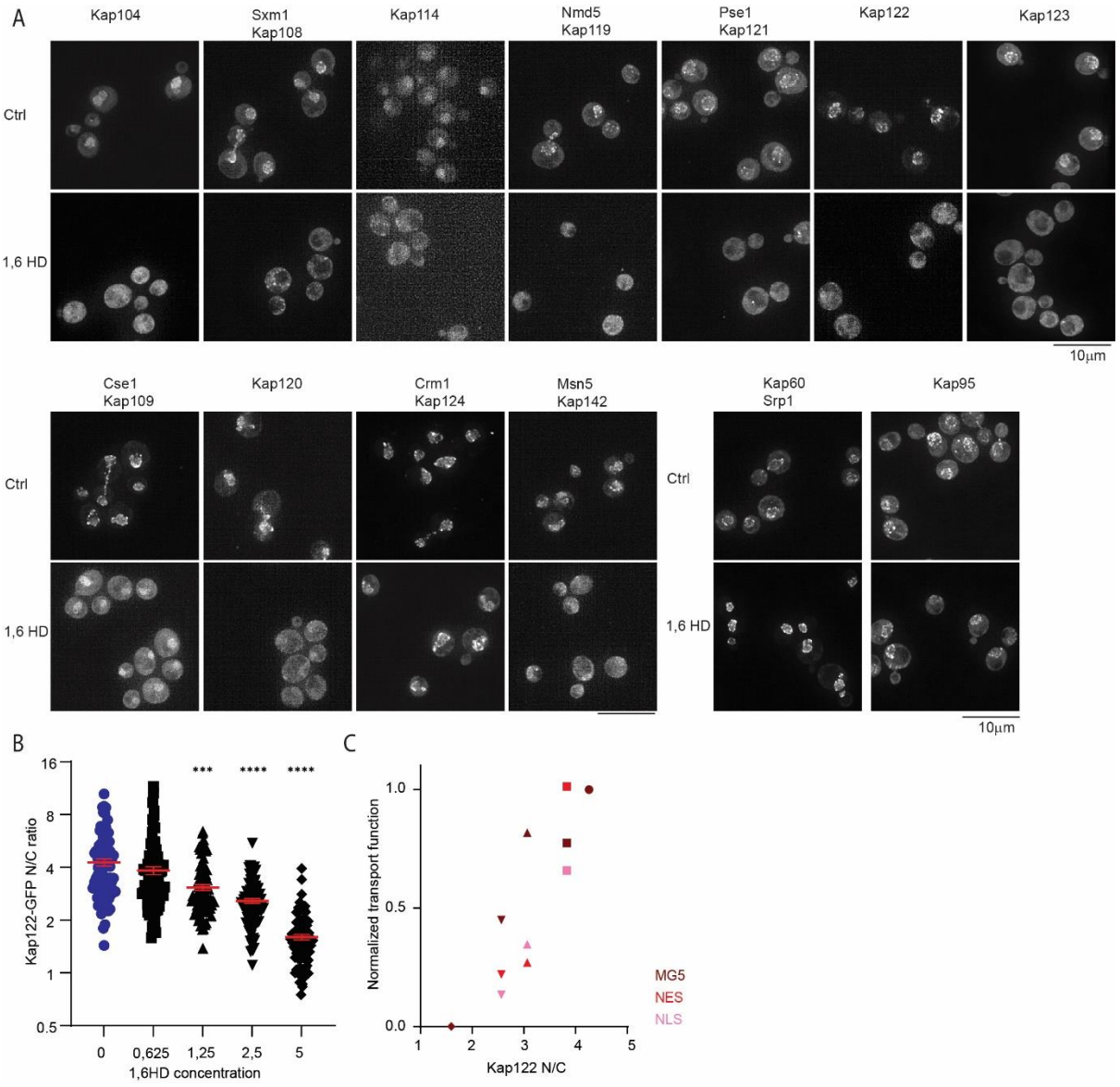

629

630 **Figure 4: Impact of 1,6HD on NTRs.** (A) Fluorescence images of endogenously GFP-tagged NTRs after
631 10 min exposure with 5% 1,6HD. Representative images of three independent replicates. The scale
632 bar is 10µm. (B) Nuclear accumulation of Kap122-GFP in yeast cells exposed for 10 min with the
633 indicated concentrations of 1,6HD. Non-parametrical Kruskal-Wallis with Dunn's multiple comparison
634 test was used to calculate statistical significance, comparing treatment to control. Error bars reflect
635 SEM from the mean of three independent experiments. 90 cells per condition were analyzed. P-values
636 ***<0,0005 ****<0,0001. (C) Average transport function measured with MG5 (dark red, normalized
637 N/C from Fig1A), GFP-NLS (pink, normalized N/C from Fig1B) and GFP-NES (red, normalized N/C from
638 Fig 1C) as a function of Kap122-GFP location at the NE and nucleus (from Fig 4B) under control
639 conditions and increasing concentrations of 1,6HD (symbols as in 4B: 0% circles; 0,625% squares;
640 1,25% triangles up; 2,5% triangles down; 5% diamonds).

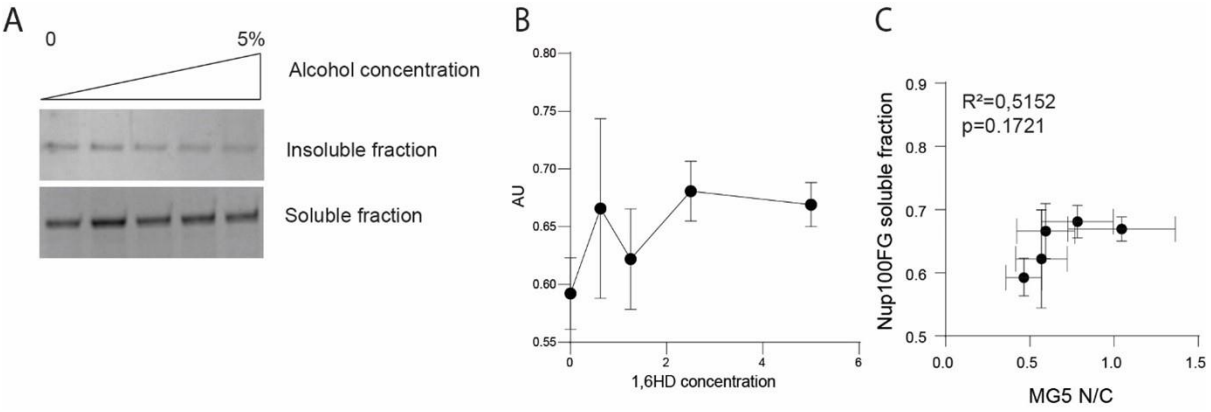

641

642 **Supplementary Figure 1.** (A) Purified Nup100FG domains were left to form condensates for 1 hour
643 and subsequently treated for 10min with 0, 0.625, 1.25, 2.5 or 5% 1,6HD. Soluble and insoluble
644 fractions were obtained by centrifugation, separated by SDS-PAGE and visualized by Brilliant Blue
645 staining. Representative image of three independent experiments. (B) Quantification of the soluble
646 fractions in (A) Error bars reflect SEM of three independent experiments. (C) Pearson correlation
647 coefficient and two-tailed P values were calculated for the N/C ratio of reporter MG5 against the
648 soluble fraction of Nup100FG domain after different concentrations of 1,6HD. Error bars reflect SEM
649 from the mean of three independent experiments.

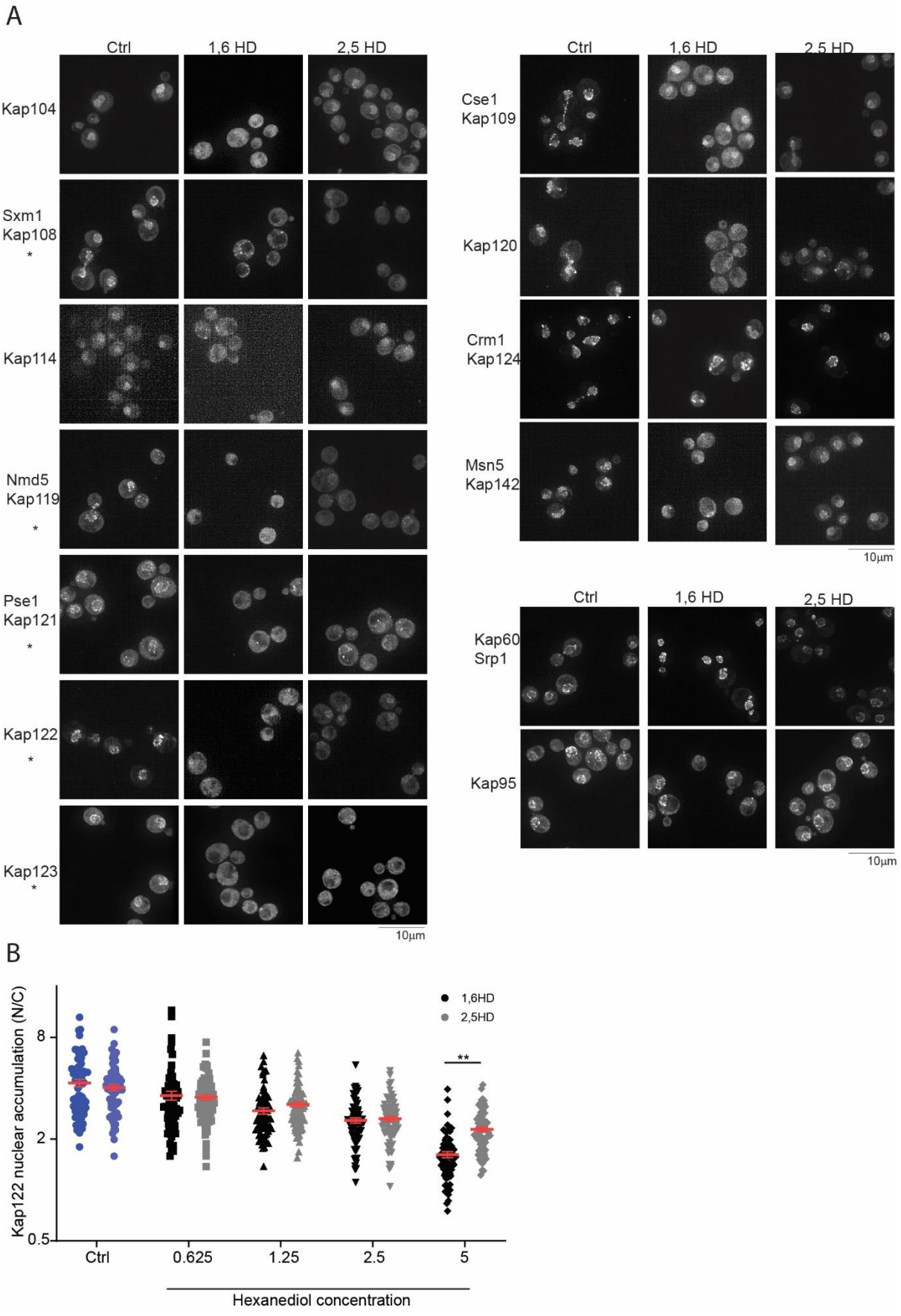

650

651 **Supplementary Figure 2** (A) Fluorescence images of endogenously GFP-tagged NTRs after 10 min
652 exposure with either 5% 1,6HD (middle, as I Fig 4A) or 5% 2,5HD (right). Representative images of
653 three independent replicates. The scale bar is 10µm. (B) Nuclear accumulation of Kap122-GFP in yeast
654 cells exposed for 10 min to the indicated concentrations of either 1,6HD (as in Fig 4B) or 2,5HD. Non-
655 parametrical Kruskal-Wallis with Dunn's multiple comparison test comparing treatment to control was
656 used to calculate statistical significance. Error bars reflect SEM from the mean of three independent
657 experiments. 70 cells per condition were analyzed. P-values **<0,005.

658

659 **Table 1: Key resources table**

Key Resources Table				
Reagent type (species) or resource	**Designation**	**Source or reference**	**Identifiers**	**Additional information**
Gene (*S. cerevisiae*)	See table 2			
strain, strain background (*S. cerevisiae*)	BY4741	Invitrogen		
strain, strain background (*S. cerevisiae*)	BY4742	Invitrogen		
strain, strain background (*S. cerevisiae*)	W303	Invitrogen		
Genetic reagent (*S. cerevisiae*)	See table 2			
Antibody	Monoclonal antibody mouse anti-GFP	Santa Cruz	sc-9996	(1:500)
Antibody	Mouse IgG kappa binding protein conjugated to HRP; m-IgGκ-BP-HRP	Santa Cruz	sc-516102	(1:10000)
Recombinant DNA reagent	See table 3			
Sequenced-based reagent	Nup60_F	This paper	PCR primers GTTGATGAAAATAAAGTTGAGGC TTTCAAGTCCCTATATACCTTTCG TACGCTGCAGGTCGAC	
Sequenced-based reagent	Nup60_R	This paper	PCR primers TTGGGCTATACGGTAATTATGTC ACGGCTAAAATTTTCATTATCAAT CGATGAATTCGAGCTCG	

Sequenced-based reagent	Nup133_F	This paper	PCR primers GAAAAAAACTATACCATCAACTA TGAAACCAACACTGTAGAATACG GTGACGGTGCTGG	
Sequenced-based reagent	Nup133_R	This paper	PCR primers CAGTAAAGTTTATTATATATATGT AAAATTGTATTATAGATATTATCG ATGAATTCGAGCTCG	
Sequenced-based reagent	Pab1_F	This paper	PCR primers GTCTTTCAAAAAGGAGCAAGAAC AACAAACTGAGCAAGCTCGTACG CTGCAGGTCGAC	
Sequenced-based reagent	Pab1_R	This paper	PCR primers GTTTGTTGAGTAGGGAAGTAGGT GATTACATAGAGCATTAATCGAT GAATTCGAGCTCG	
chemical compound, drug	Yeast extract	BD	291946	
chemical compound, drug	Complete supplement mixture complete	Formedium	DCS0019	
chemical compound, drug	D-Glucose anhydrous	Fisher Chemical™	10141520	
chemical compound, drug	D-Raffinose pentahydrate	Thermo Scientific	195675000	
chemical compound, drug	D-Galactose	Acros Organics	150610010	
chemical compound, drug	Phosphatase buffered saline	Sigma-Aldrich	P4417	
chemical compound, drug	Tris base	Fisher Scientific™	BP152-1	
chemical compound, drug	HEPES	Fisher Scientific™	BP310-500	
chemical compound, drug	Sodium dodecyl sulfate (SDS) solution, 20%	SERVA	20767.03	

chemical compound, drug	EDTA	Sigma-Aldrich	ED2P-500	
chemical compound, drug	Triton X-100	Acros Organics	215682500	
chemical compound, drug	2-mercaptoethanol	Sigma-Aldrich	M6250-100	
chemical compound, drug	Sodium chloride	Acros Organics	207790010	
chemical compound, drug	Tween20	MP Biomedicals	TWEEN201	
chemical compound, drug	Magnesium chloride hexahydrate	Sigma-Aldrich	M2393	
chemical compound, drug	Sodium acetate anhydrous	Fisher Chemical™	S2080/53	
chemical compound, drug	Magnesium acetate tetrahydrate	Fisher Scientific™	BP215	
chemical compound, drug	Glycerol	Sigma-Aldrich	G5516	
chemical compound, drug	Phenylmethanesulfonyl fluoride (PMSF)	Sigma-Aldrich	P7626	
chemical compound, drug	cOmplete ULTRA tablets, Mini EDTA-free	Roche	05892791001	
chemical compound, drug	Albumine bovine serum (BSA)	Acros Organics	268131000	
chemical compound, drug	Glass beads	BioSpec Products	11079105	
chemical compound, drug	PierceTM BCA Protein Assay Kit	Fisher Scientific™	23225	

chemical compound, drug	ECL Prime Western Blotting Detection Reagent	Amersham	RPN2232	
chemical compound, drug	GX Stain-Free™ FastCast™ Acrylamide Kit, 10%	BioRad	1610183	
chemical compound, drug	PVDF Transfer Membrane	Thermo Scientific	88518	
chemical compound, drug	Methanol Technical	VWR	20903.368	
chemical compound, drug	IPTG	Sigma-Aldrich	10724815001	
chemical compound, drug	Ni sepharose	Cytiva	17531802	
chemical compound, drug	Guanidine hydrochloride	Thermo Scientific	24110	
chemical compound, drug	Brilliant blue G	Sigma-Aldricht	G-250	
chemical compound, drug	1,6 hexandiol	Sigma-Aldricht	240117-50	
chemical compound, drug	2,5 hexandiol	Sigma-Aldricht	H11904-50	
chemical compound, drug	Sodium azide	Sigma-Aldricht	S2002-100	
chemical compound, drug	2-deoxy-d-glucose	Sigma-Aldricht	D8375-1	
software, algorithm	Fiji	(Schindelin et al. 2012)		
software, algorithm	Resolve3D SoftWoRx	Cytiva		

661 Table 2 Yeast strains used in this publication

Strain BY4741 [1]	Genotype	Source
yPP008; GFP-tcNLS	Mata his3Δ1 leu2Δ0 met15Δ0 ura3Δ0 GFP-tcNLS(pGal1)::His Nup49-mCh::URA	(Rempel et al. 2019)
yPP011; GFP-NES	Mata his3Δ1 leu2Δ0 met15Δ0 ura3Δ0 GFP-NES(pGal1)::His Nup49-mCh::URA	(Rempel et al. 2019)
GFP collection [2)]	Mata his3Δ1 leu2Δ0 met15Δ0 ura3Δ0 **XX**-GFP::HIS3M X 6	ThermoFisher
Nup116-GFPboundary	Mata his3Δ1 leu2Δ0 met15Δ0 ura3Δ0	(Rempel et al. 2019)
yER016; Nup60-GFP [1)]	Mata leu2-3, 112 trp1-1 can1-100 ura3-1 ade 2-1 his3-11, 15 Nup60-GFP::KanMX4	This paper
yIS010; Nup2-GFP Nup49mCherry	Mata his3Δ1 leu2Δ0 met15Δ0 ura3Δ0 Nup2-GFP::His3MX6 Nup49-mCherry::URA	(Rempel et al. 2019)
yER020; Pab1-GFP	Mata his3Δ1 leu2Δ0 met15Δ0 ura3Δ0 Pab1-GFP::HIS3M X 6	This paper
RFP localization database [3)]	Matα his3Δ1 leu2Δ0 lys2Δ0 ura3Δ0 **YY**-RFP::KanMX6	(Huh et al. 2003)
SMY15	Mata his3Δ1 leu2Δ0 met15Δ0 ura3Δ0 pTEF1-pHluorin::His3M X 6	(Mouton et al. 2020)
SMY16	Mata his3Δ1 leu2Δ0 met15Δ0 ura3Δ0 ATP sensor pTEF1-his6-ymEGFP Δ11-B.subtilis ε-ymScarletI::HIS3M X 6	(Semmelink et al. 2022)
yER023; Kap122-GFP Nup133mCherry	Mata his3Δ1 leu2Δ0 met15Δ0 ura3Δ0 Kap122-GFP::HIS3M X 6 Nup133-mCherry::URA	This paper

1) yER016 is in W303 background
2) **XX** is: NSP1, Nup49, Nup100, Nup133, Nup159, Nup170, LSM4, Hsp104, ATP1, Get1, Vma1, Pma1, Tub1, Kap124, Kap95, Kap60, Kap122, Kap104, Kap142, Kap119, Kap121, Kap108, Kap109, Kap114, Kap120, Kap123.
3) **YY** is: Anp1, Pex3, Nop56, Erg6, Snf7.

662

663 Table 3 Plasmids used in this publication.

Plasmid number	Genotype	Source
pPP008; MG5	pUG34-Gal1-MBP-5XGFP-His	(Popken et al. 2015)
pACM063; mCh-L-TM	pUG36-Gal-mCherry linker-TM-URA	(Meinema, Poolman, and Veenhoff 2013)
pYM28	pAgTEF-SpHIS5-tAgTEF	Euroscarf, Janke et al 2004
pYM30	pAgTEF-kanMX-tAgTEF	Euroscarf, Janke et al 2004
pPP014	mCherry-Ura cassette	(Rempel et al. 2019)

664